Int. J. Heat Mass Transfer. Vol. 36, No. 5, pp. 1181–1189, 1993
Printed in Great Britain

0017-9310/93 $6.00+0.00

Three-dimensional radiation in absorbing–emitting–scattering media using the modified differential approximation

H. M. PARK, R. K. AHLUWALIA and K. H. IM
Argonne National Laboratory, 9700 South Cass Avenue, Argonne, IL 60439, U.S.A.

(*Received* 20 *February* 1992 *and in final form* 5 *June* 1992)

Abstract—The modified differential approximation (MDA) first proposed by Olfe and recently extended by Modest is applied to a three-dimensional absorbing–emitting–scattering medium bounded by non-black walls. Numerical techniques are developed to solve for the radiation fields due to wall emission and medium emission. The techniques are evaluated in terms of the computer memory requirement, CPU time and numerical accuracy. For a model problem, the modified differential approximation is compared against the zone method, the P_1 approximation, the P_3 approximation, S_4 and S_6. MDA is shown to be superior to the P_1 and P_3 approximations and to compare favorably with S_N solutions for all conditions of optical depth.

1. INTRODUCTION

THE DIFFERENTIAL approximation, also known as the moment method or P_1 approximation, is a popular technique of solving the radiation transport equation for absorbing, emitting and scattering media. Although it is accurate in optically thick situations, it becomes unacceptable in optically thin situations, particularly for multi-dimensional media. One way of extending the optical thickness range in which the differential approximation remains valid is to retain higher order terms in the Legendre polynomial expansion of the radiation intensity. The resulting higher order approximations, such as P_3 and P_5, are considerably more involved but still inaccurate for sufficiently small optical thickness.

In a series of papers, Olfe [1–3] offered an alternative approach to improving the accuracy of the P_1 approximation. The approach, called modified differential approximation (MDA), consists of separating the wall emission from the medium emission. Recently, Modest [4] demonstrated that Olfe's MDA may be formulated for a general absorbing, emitting and anisotropically scattering medium bounded by diffusely emitting and reflecting walls. He presented MDA solutions of a one-dimensional slab at radiative equilibrium and a two-dimensional cold cylinder with isotropic scattering. He compared the solutions with Olfe's slab analysis, the ordinary P_1 solution for a cold cylinder and the exact Monte Carlo solution to show that MDA yields results of excellent accuracy for all optical conditions.

The purpose of this paper is to apply Modest's formulation of MDA to a three-dimensional absorbing, emitting and scattering medium bounded by non-black walls. The major emphasis is on development of numerical techniques for determining radiation fields due to wall emission and medium emission, characterization of techniques with regard to computational speed and memory requirements, and comparison of three-dimensional MDA solutions to those obtained from the zonal method, the higher order differential approximation and discrete-ordinate methods.

2. THEORY

For a three-dimensional absorbing, emitting and scattering rectangular enclosure, the radiation transport equation is

$$\nabla\cdot(\hat{s}I)+\beta I=(1-\omega)\beta I_b+\frac{\omega\beta}{4\pi}\int_{4\pi}I(\mathbf{r},\hat{s}')\phi(\hat{s},\hat{s}')\,\mathrm{d}\Omega' \tag{1}$$

where I is the spectral radiation intensity in the beam direction $\hat{s}$, β and ω are, respectively, the spectral extinction coefficient and scattering albedo, I_b is the Planck function, ϕ is the scattering phase function and Ω denotes the solid angle. Following Modest [4], we decompose the radiation intensity I into two parts: one, I_s, that may be traced to emission from the enclosure walls, and the second, I_m, that may be traced to emission from the medium. The two components of intensity are governed by the following equations:

$$\nabla\cdot[\hat{s}I_s(\mathbf{r},\hat{s})]+\beta I_s(\mathbf{r},\hat{s})=0 \tag{2}$$

and

$$\nabla\cdot[\hat{s}I_m(\mathbf{r},\hat{s})]+\beta I_m(\mathbf{r},\hat{s})=(1-\omega)\beta I_b+\frac{\omega\beta}{4\pi}\int_{4\pi}I(\mathbf{r},\hat{s}')\phi(\hat{s},\hat{s}')\,\mathrm{d}\Omega'. \tag{3}$$

The I_s field, given by equation (2), accounts for radi-

NOMENCLATURE

a_1	anisotropic scattering coefficient	ε	emissivity
A	surface area	ϕ	scattering phase function
F	view factor	τ	optical thickness
gs	exchange coefficient	ω	scattering albedo
G	incident radiation	Ω	solid angle.
I	intensity		
J	radiosity		
$\mathbf{q}$	heat flux		
$\hat{s}$	beam direction	Subscripts	
T	temperature.	b	black body
		m	medium-originated radiation
Greek symbols		s	surface-originated radiation
β	extinction coefficient	w	wall.

ation emitted by the enclosure walls after attenuation by medium absorption and scattering and by wall reflections. It admits the following solution:

$$I_s(\mathbf{r},\hat{s}) = \frac{J_w(\mathbf{r}')}{\pi} e^{-\tau}, \quad \tau = \int_0^s \beta \, ds' \tag{4}$$

where J_w is the radiosity at the wall from where the beam emanates and τ is the optical distance between that point on the wall (r') and the point under consideration (r). The wall radiosity J_w is determined in the usual manner as the sum of wall emission and reflection

$$J_w(\mathbf{r}') = \varepsilon_w \pi I_{bw}(\mathbf{r}') + (1-\varepsilon_w)\int_A J_w(\mathbf{r}') \frac{\cos\theta \cos\theta'}{\pi|\mathbf{r}-\mathbf{r}'|^2} e^{-\tau} dA. \tag{5}$$

In equation (5), ε_w is the spectral wall emissivity, following Modest [4], whereas I_s, with its origin from the radiation emitted by the wall, has a highly irregular angular distribution, I_m, with its origin linked to medium emission, is expected to be near isotropic. Thus, equation (3) describing I_m can be simplified by applying the P_1 approximation. For a linear anisotropic phase function

$$\phi(\hat{s},\hat{s}') = 1 + a_1 \hat{s}\cdot\hat{s}' \tag{6}$$

the incident radiation G_m is given by the following equation:

$$\nabla\cdot\frac{1}{\beta_1}\nabla G_m - 3(1-\omega)\beta G_m = -12\pi(1-\omega)\beta I_b - 3\omega\beta\left[1+\frac{a_1}{3(1-\omega_1)}\right]G_s \tag{7}$$

where

$$\beta_1 = \beta(1-\omega_1)$$

and

$$\omega_1 = a_1\omega/3. \tag{8}$$

For a diffusely reflecting surface, G_m admits Marshak's boundary conditions for a cold surface

$$-\frac{\gamma}{\beta_1}\hat{n}\cdot\nabla G_m + G_m = -\frac{3\gamma\omega_1}{1-\omega_1}\mathbf{q}_s\cdot\hat{n} \tag{9}$$

where

$$\gamma = \frac{2}{3}\left(\frac{2}{\varepsilon_w}-1\right). \tag{10}$$

Finally, in solving the energy equation, knowledge of the specific gas cooling rate due to thermal radiation is required and is given as

$$\nabla\cdot\mathbf{q} = 4\pi(1-\omega)\beta\left(I_b - \frac{G_m+G_s}{4\pi}\right). \tag{11}$$

As pointed out by Modest, the MDA reduces to the correct limit for the optically thin as well as the optically thick media. In the thin limit, the medium emission-related contribution to heat transfer vanishes. In the thick limit, the MDA solution converges to the P_1 approximation.

3. NUMERICAL SOLUTION

Our numerical technique is geared to obtain the $\nabla\cdot\mathbf{q}$ distribution within the medium and the wall heat flux distribution. The overall solution is obtained in three steps. In the first step, equation (5) is solved numerically for the wall radiosity distribution. The second step consists of integrating equation (4) for incident radiation G_s and wall heat flux $\mathbf{q}_s$. These two variables constitute inputs to equation (7), which is solved for G_m and $\mathbf{q}_m$ by a finite difference technique. For numerical purposes, the rectangular furnace is subdivided into a uniform $I\times J\times K$ grid.

3.1. *Radiosity distribution*

Equation (5) is equivalent to an enclosure problem for a participating medium. It is a Fredholm integral

equation which may be approximated by the following set of algebraic equations:

$$J_{wl} = \varepsilon_{wl}\pi I_{bwl} + (1-\varepsilon_{wl}) \sum_{m=0}^{N} J_{wm} F_{lm} \qquad (12)$$

where l is a wall segment, $N = 2(I\times J + J\times K + K\times I)$, and F_{lm} represents the view factor between wall segments l and m separated by the participating medium

$$F_{lm} = \frac{1}{A_l}\int_{A_l}\int_{A_m} \frac{\cos\theta\cos\theta'}{\pi|\mathbf{r}-\mathbf{r}'|^2} \times \exp(-\beta|\mathbf{r}-\mathbf{r}'|)\,dA_l\,dA_m. \qquad (13)$$

For small β or when segments l and m are in close proximity, fine subdivisions are required to estimate F_{lm} accurately. The computational effort can be greatly relieved by likening F_{lm} to the surface exchange area $\bar{S}_i\bar{S}_j$ used in the zone method. Tucker [5] has derived exponential correlations for direct exchange areas between square surfaces. For perpendicularly oriented surfaces of grid size B separated by distances X, Y and Z on remote corners, Table 1 presents the coefficients for use in the following exponential correlation:

$$F_{lm} = C\exp(-A\tau_\beta), \quad \tau_\beta = \beta B,$$
$$A = A_0 + A_1\tau_B + A_2\tau_B^2 + A_3\tau_B^3 + A_4\tau_B^4. \qquad (14)$$

Outside the range of the correlation, i.e. X/B, Y/B or $Z/B > 3$, single-point quadrature is employed for calculating F_{lm} from equation (13). Tucker also presents exponential correlations for parallel square surfaces. These are not useful in the present work since the normalized separation X/B, Y/B or Z/B for parallel surfaces is invariably larger than 4 so that single-point quadrature is sufficiently accurate.

Equation (12) represents a set of $2(I\times J + J\times K + K\times I)$ linear algebraic equations that is easily inverted by the method of successive substitutions. Generally, three to five iterations are sufficient to obtain a convergent solution with a relative error in J_w smaller than 10^{-10}. View factors F_{ij} are calculated once and stored as read only memory (ROM).

3.2. *Incident radiation* G_s

A formal solution of the G_s field can be constructed by integrating I_s, given by equation (4), over the solid angle

$$G_s(\mathbf{r}) = \frac{1}{\pi}\int_{4\pi} J_w \exp(-\beta|\mathbf{r}-\mathbf{r}'|)\,d\Omega. \qquad (15)$$

An obvious way of performing solid angle integration is to subdivide the enclosure wall into small area elements δA_w and conduct the following summation:

$$G_s(\mathbf{r}) = \sum \frac{J_w}{\pi}\exp(-\beta|\mathbf{r}-\mathbf{r}_w|)\frac{\cos\theta\delta A_w}{|\mathbf{r}-\mathbf{r}_w|^2}. \qquad (16)$$

The foregoing summation represents a one-point quadrature. It has proved unsatisfactory for two reasons. First, the quadrature method is very inaccurate for field points in close proximity to the wall elements. A proper error control was found to require an excessively large number of surface grid points. Second, equation (16) yields G_s at a specific field point, whereas a volume-averaged quantity is required in solving equation (7) for G_m. The latter can be obtained by performing the following five-fold integration with a sufficient number of quadrature points:

$$G_s = \frac{1}{\Delta V}\int\int\int_{\Delta V}\int\int_{A_w} \frac{J_w}{\pi}\exp(-\beta|\mathbf{r}-\mathbf{r}_w|) \times \frac{\cos\theta}{|\mathbf{r}-\mathbf{r}_w|^2}\,dA_w\,dV. \qquad (17)$$

The computational effort expended in evaluating the multi-dimensional integral can be greatly reduced by

Table 1. Tucker's correlation coefficients for exchange areas between perpendicularly oriented surfaces; see equation (14)

X/B	Y/B	Z/B	C	A_0	A_1	A_2	A_3	A_4
1	1	1	0.2000	0.5390	−0.0615	0.00429	−0.000151	0.206E−5
2	1	1	0.0406	0.9965	−0.0878	0.00419	−0.773E−4	0
3	1	1	0.0043	1.906				
1	2	1	0.0328	1.571	−0.0391	0.00208		
2	2	1	0.0189	1.751				
3	2	1	0.0059	2.384				
1	3	1	0.0089	2.502				
2	3	1	0.0069	2.665				
3	3	1	0.0036	3.129				
1	2	2	0.0329	2.055				
2	2	2	0.0230	2.245				
3	2	2	0.0101	2.780				
1	3	2	0.0159	2.860				
2	3	2	0.0129	3.010				
3	3	2	0.0076	3.435				
1	3	3	0.0124	3.481				
2	3	3	0.0107	3.609				
3	3	3	0.0073	3.976				

expressing the integral in terms of the gas–surface exchange area $\overline{gs}$ used in the zone method

$$G_s = \frac{1}{\Delta V}\sum_{m=0}^{N}\frac{J_w}{\beta}\overline{gs} \tag{18}$$

$$\overline{gs} = \int_{A_w}\int_{\Delta V}\beta\exp(-\beta|\mathbf{r}-\mathbf{r}_w|)\frac{\cos\theta}{\pi|\mathbf{r}-\mathbf{r}_w|^2}\,dA_w\,dV \tag{19}$$

where Tucker [5] has presented the following exponential correlations for estimating the surface–volume exchange areas between cubic gas zones and square surface zones:

$$\overline{gs}/(\overline{gs})_b = C\exp(-A\tau_B),\quad \tau_B = \beta B$$
$$A = A_0 + A_1\tau_B + A_2\tau_B^2$$
$$(\overline{gs})_b = 4\beta B^3\exp(-0.43288\tau_B + 0.042148\tau_B^2 - 0.0023416\tau_B^3 + 0.000050513\tau_B^4). \tag{20}$$

Table 2 presents the correlation coefficients for normalized separation distances X/B, Y/B and $Z/B < 3$. A single-point quadrature is used for evaluating $\overline{gs}$ from equation (19) when the normalized separation distance is larger than 3.

Consistency and accuracy of the numerical solutions for J_w and G_s can be verified by integrating the I_s transport equation (2) over the solid angle and applying the divergence theorem

$$\int\nabla\cdot\mathbf{q}_s\,dV + \int\beta G_s\,dV = \int\mathbf{q}_s\cdot\hat{n}\,dA + \int\beta G_s\,dV = 0 \tag{21}$$

where

$$\int\mathbf{q}_s\cdot\hat{n}\,dA = -\sum J_{wl}A_l + \sum\sum J_{wl}F_{lm}A_l. \tag{22}$$

We can define a factor f as the ratio of radiation attenuated in the medium and reaching the enclosure walls unattenuated to the total radiation leaving the enclosure walls

$$f = \sum\sum\frac{J_{wl}F_{lm}A_l + \int\beta G_s\,dV}{\sum J_{wl}A_l}. \tag{23}$$

If the numerical solution were exact, f would be unity. Deviation of f from unity is a measure of inaccuracy in G_s computation and the enclosure problem. In one of the numerical experiments, use of Tucker's exponential correlation for exchange areas yielded a value of 1.00172 for f when a uniform $5\times5\times10$ grid was applied to a $2\times2\times4$ m furnace with β equal to 0.5.

3.3. G_m field

Equation (7) for G_m subject to the boundary condition given by equation (10) can be easily discretized by finite differencing. We adopt a conservative scheme in which discretization is performed by integrating the governing equation over the control volume. A cell-centered finite difference approximation is used for the derivative term and a cell-averaged approximation for the remaining terms. Auxiliary grids are defined for application of the boundary conditions and evaluation of derivatives at the boundaries. On collecting the coefficients of the discretized equations, the following set of algebraic equations is obtained:

$$A^P G_{mijk} = A^E G_{mi+1jk} + A^W G_{mi-1jk} + A^N G_{mij+1k} + A^S G_{mij-1k} + A^H G_{mijk+1} + A^L G_{mijk-1} + S_{ijk}$$

where for internal points

$$A^E = \Delta y_j\Delta z_k/(\beta_{1i+1/2jk}\Delta x_{i+1/2})$$
$$A^W = \Delta y_i\Delta z_k/(\beta_{1i-1/2jk}\Delta x_{i-1/2})$$
$$A^N = \Delta x_i\Delta z_k/(\beta_{1ij+1/2k}\Delta y_{j+1/2})$$
$$A^S = \Delta x_i\Delta z_k/(\beta_{1ij-1/2k}\Delta y_{j-1/2})$$

Table 2. Tucker's correlation coefficients for exchange area between cubic gas zones and square surface zones; see equation (20)

X/B	Y/B	Z/B	C	A_0	A_1	A_2
2	1	1	0.0337	0.4563	−0.0311	0.824E−3
3	1	1	0.0048	1.457		
2	2	1	0.0137	0.8332	−0.0469	−0.00103
3	2	1	0.0034	1.674		
3	3	1	0.0017	2.251		
1	1	2	0.0313	1.062		
2	1	2	0.0200	1.292		
3	1	2	0.0078	1.933		
2	2	2	0.0135	1.514		
3	2	2	0.0062	2.089		
3	3	2	0.0037	2.602		
1	1	3	0.0120	2.033		
2	1	3	0.0098	2.210		
3	1	3	0.0060	2.666		
2	2	3	0.0083	2.366		
3	2	3	0.0053	2.806		
3	3	3	0.0037	3.201		

$$A^{H} = \Delta x_i \Delta y_j / (\beta_{ijk+1/2} \Delta z_{k+1/2})$$

$$A^{L} = \Delta x_i \Delta y_j / (\beta_{ijk-1/2} \Delta z_{k-1/2})$$

$$A^{P} = A^{E} + A^{W} + A^{N} + A^{S} + A^{H} + A^{L} + 3(1-\omega_{ijk})\beta_{ijk}\Delta x_i \Delta y_j \Delta z_k$$

$$S_{ijk} = 12\pi(1-\omega_{ijk})\beta_{ijk} I_{bijk} \Delta x_i \Delta y_j \Delta z_k + 3\omega_{ijk}\beta_{ijk}[1 + a_{ijk}/3(1-\omega_{ijk})] G_{sijk} \Delta x_i \Delta y_j \Delta z_k. \quad (24)$$

Three different methods have been attempted for solving the foregoing set of algebraic equations: a successive over-relaxation method (SOR), an iterative line-by-line elimination procedure based on the tridiagonal matrix inversion algorithm (TDMI), and sparse matrix inversion package developed at Yale University (YSMP). With the introduction of an optimal over-relaxation parameter, determined by experiments, TDMI has been found to be two to three times faster than the optimal SOR. Both TDMI and SOR are found to suffer slow convergence at small extinction coefficient β. For coarse grids with less than 1000 nodes, YSMP is 10–100 times faster than TDMI. For fine grids and enclosures with non-unit aspect ratios, the memory requirement of YSMP becomes excessively large and the computational speed advantage over TDMI also begins to disappear. Finally, since the finite difference scheme is conservative, the Gauss theorem can be employed to establish a convergence criterion for the iteration procedure

$$\iiint \nabla \cdot \mathbf{q} \, dV = \iint \mathbf{q} \cdot \hat{n} \, dA_w = \iiint 4\pi(1-\omega)\beta \left(I_b - \frac{G_m + G_s}{4\pi} \right) dV. \quad (25)$$

4. COMPUTATIONAL BEHAVIOR

As mentioned earlier, the view factor array F_{lm} is not assigned to random access memory (RAM). For a $20 \times 20 \times 20$ grid, the array is 5.96 Mb words long and is more conveniently stored as read only memory (ROM). One consequence of using ROM storage is increased I/O time. For maximum economy in I/O time, unformatted storage is used for F_{lm} and all search procedures are avoided by reading F_{lm} in the order it is written. The array size can be halved by using the reciprocity relation $F_{lm} = A_m F_{ml}/A_l$. For constant β and for certain restrictive variations in β, the array size can be further reduced from similarity arguments.

Timing tests have been conducted to quantify the computational effort expended in the three major segments of MDA: the enclosure problem, G_s field and G_m field. For the purpose of these tests, wall and gas temperatures are assumed to be given. Table 3 provides a breakdown of CPU times on a SUN SPARC SLC workstation for $4 \times 4 \times 14$, $8 \times 8 \times 28$, $12 \times 12 \times 42$ and $16 \times 16 \times 56$ grids. The majority of CPU time is seen to be incurred in subroutines dedicated to determining J_w and G_s fields. For a cubic enclosure, the CPU time for the G_m field scales up with the number of grid points as I^3, as I^4 for the J_w field and as I^5 for the G_s field. The scaling order implies that from a computational standpoint, MDA becomes increasingly inefficient as the grid system is refined.

Table 3. Breakdown of CPU time (s) on SUN SPARC SLC

Grid	MDA			Improved MDA	
	J_w	G_s	G_m	G_s	G_m
$4 \times 4 \times 14$	47	28.4	0.3	5.5	0.4
$8 \times 8 \times 28$	1142	1473.6	2.6	23.7	2.6
$12 \times 12 \times 42$	5045	10093	5.9	63.5	8.8
$16 \times 16 \times 56$	26450	75483	20	132.7	20.7

From the foregoing discussion there is a clear incentive to seek an alternative formulation for the G_s field that avoids I^4 and I^5 scaling of CPU time. We have applied the discrete ordinate (S_4) technique to equation (2) for G_s. The S_4 solution for G_s is particularly expedient since equation (2) contains no terms for medium emission and in-scattering. The CPU time for improved MDA, i.e. $S_4 + P_1$, is compared to regular MDA (Modest's formulation) in Table 3. An impressive reduction in CPU time—ranging from a factor of 14 for a $4 \times 4 \times 14$ grid to 768 for a $16 \times 16 \times 56$ grid—is obtained. More details of the computational aspects of the improved MDA formulation will be presented as a technical note in a future publication.

In a problem with specified wall temperature and temperature-independent radiation properties, the radiosity distribution and the G_s field (or alternatively the S_4 solution for G_s) need to be determined only once. The G_m field must be determined iteratively in conjunction with the solution of the energy equation for the temperature field. For 6–10 temperature iterations, the total CPU time in the improved MDA formulation for G_s becomes comparable to that for the G_m (P_1) solution. Thus, with a modest increase in computational effort, the improved MDA formulation expands the validity of the P_1 approximation, which is normally applicable only in the optically-thick limit, to the entire range of the optical spectrum.

5. COMPARISON WITH OTHER METHODS

For the purpose of validating MDA, we select a simple problem that has been analyzed by many investigators using different methods. The enclosure to be analyzed is a rectangular box of dimensions 2 m (X), 2 m (Y) and 4 m (Z). The temperature boundary conditions are: 1200 K at $z = 0$, 400 K at $z = 4$ m and 900 K for all other walls. Surface emissivity is specified as 0.85 for wall $z = 0$ and 0.70 for all other walls. The medium is gray with a constant 5 kW m^{-3} volumetric

heat source ($\nabla \cdot \mathbf{q}$). With divergence of heat flux specified, it is not necessary to solve for the temperature field explicitly since the Planck function I_b can be eliminated from the G_m equation by combining equations (7) and (11)

$$\nabla \cdot \frac{1}{\beta_t} \nabla G_m = 3\nabla \cdot \mathbf{q} - \frac{3\beta}{(1-\omega_t)} G_s. \tag{26}$$

The solution for the P_1 approximation can be obtained from equation (26) by setting G_s equal to zero and modifying the boundary conditions given by equation (9) as

$$-\frac{\gamma}{\beta_t} \hat{n} \cdot \nabla G_m + G_m = 4\pi I_w. \tag{27}$$

Figure 1 compares the temperature distribution in the rectangular enclosure at two different heights for various values of the extinction coefficient β. For purposes of comparison, results from the zone method, P_N approximations and S_N approximations are also presented in this figure. One difficulty in directly comparing different models stems from the dissimilarity in grids requiring linear interpolation of calculated temperatures and heat fluxes between the grid nodes. Our MDA and P_1 calculations are based on a $5 \times 5 \times 10$ uniform grid used in the zonal method. Mengüc and Viskanta [6] have employed a $7 \times 7 \times 11$ grid in their work on the P_3 approximation. Truelove [7] performed his S_4 calculations on an $8 \times 8 \times 15$ grid. Assuming that the zone method provides the most exact solution, Fig. 1 shows that MDA is accurate near the cold wall ($z = 3.6$ m) and reasonably accurate in the vicinity of the hot wall ($z = 0.4$ m). Near the hot wall, MDA has accuracy comparable to the P_3 approximation and better than the P_1 approximation. The accuracy of MDA is somewhat independent of the optical thickness whereas that of the P_1 and P_3 solutions deteriorates as the optical thickness decreases.

Figure 2 exhibits the heat flux profiles at the top (cold) and bottom (hot) walls. The general trend is that the P_1 and P_3 solutions significantly overestimate the heat flux. (The exception is the P_1 solution at $z = 0$ for $\beta = 1.0\ m^{-1}$, but this seems to be a coincidence.) As expected, the accuracy of P_N solutions improves as the optical thickness increases, but the prediction of heat flux for an optically thin medium ($\beta = 0.25$ and $0.5\ m^{-1}$) is unacceptably poor. On the contrary, MDA yields an almost exact heat flux at the cold wall ($z = 4$ m) and an accurate prediction at the hot wall, especially at the boundaries, $x = 0.2$ m. Here again, the accuracy of MDA is insensitive to the magnitude of the extinction coefficient.

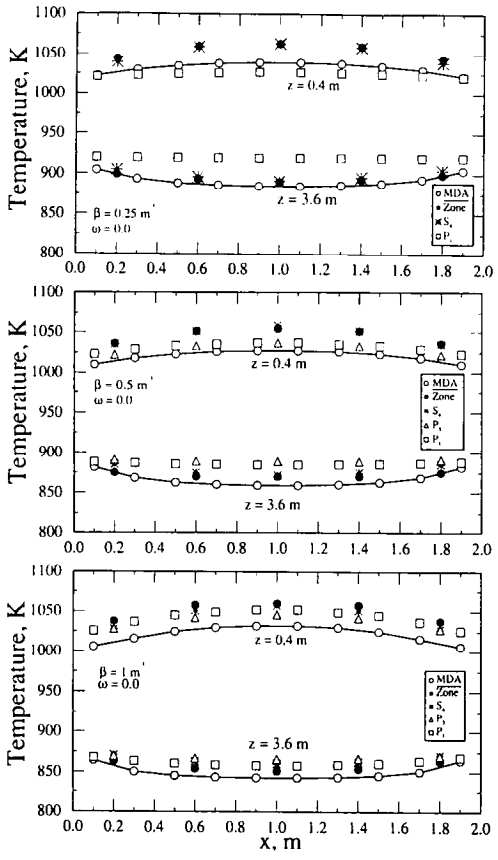

FIG. 1. Comparison of gas temperature fields calculated from MDA, zone, P_1, P_3, and S_4 methods: purely absorbing medium.

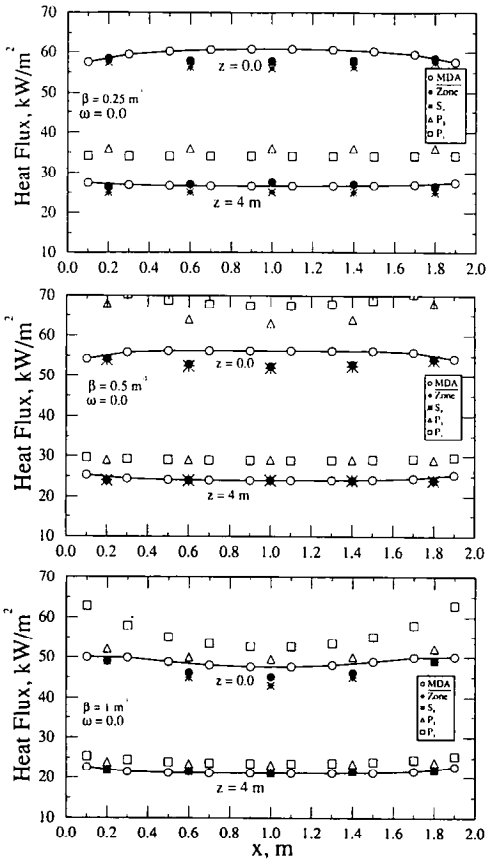

FIG. 2. Comparison of heat flux calculated from MDA, zone, P_1, P_3 and S_4 methods: purely absorbing medium.

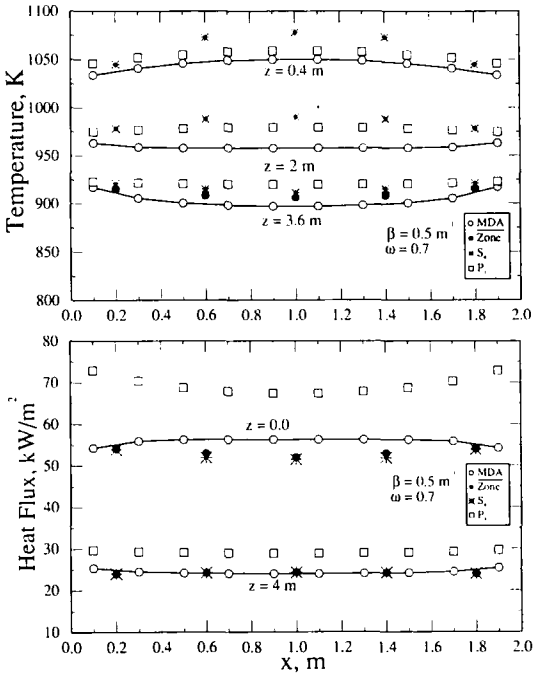

FIG. 3. Comparison of temperature field and heat flux calculated from MDA, zone, P_1 and S_4 methods: isotropically scattering medium.

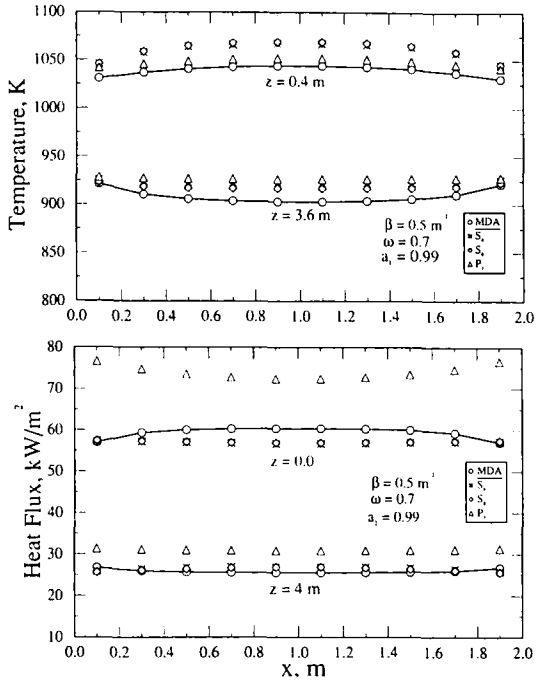

FIG. 4. Comparison of temperature field and heat flux calculated from MDA, P_1, S_4 and S_6 methods: anisotropically scattering medium.

Figure 3 shows the effect of isotropic scattering ($\omega = 0.7$) on the temperature and heat flux profiles. The general trends are similar to the case without scattering. The modified differential approximation yields better results than the P_1 solution near the walls, but the temperature distribution determined from MDA has about 1% error in the center of the enclosure. As explained by Truelove [7], the effect of isotropic scattering is to increase the emissive power σT^4 by $\omega \nabla \cdot \mathbf{q}/4\beta(1-\omega)$, while the heat flux distribution is unchanged for the specified radiative flux in the medium. The present numerical results from the modified differential approximation and the P_1 approximation give results consistent with this explanation, i.e. the heat flux distribution almost remains unchanged whereas the temperature increases uniformly throughout the enclosure. However, for more general boundary conditions where the temperature field in the medium is specified or the temperature distribution is obtained simultaneously with the radiation intensity, the effect of scattering on the heat flux is usually significant.

Figure 4 shows the effect of anisotropic scattering on the temperature and heat flux profiles. The forward scattering ($a_1 = 0.99$) increases the absolute value of the heat flux by about 10% when the extinction coefficient is 0.5 and the albedo is 0.7. For the same values of these parameters, the temperature profiles are almost the same as the isotropic scattering case ($a_1 = 0$). The heat flux increases with a_1 since the forward scatter enhances the heat transfer from hot to cold walls. As the albedo increases, the effect of the forward scattering is expected to grow because of the dominance of scattering in radiation transport.

6. DISCUSSION AND CONCLUSION

The MDA has the appealing attribute of being physically correct in the optically thin and thick limits. Various merits, limitations and characteristics of MDA are evaluated below with the help of some illustrative examples.

(a) In the optically thin limit, the G_s field serves as the correct solution to the radiation transport equation. In this limit, the accuracy of the MDA solution is determined by the numerical accuracy to which equation (2) is solved. To elucidate this point, P_1, MDA, S_4 and S_6 methods have been applied to the problem posed in Section 5 with $\beta = 0.1\ \mathrm{m}^{-1}$, $\omega = 0.7$ and $a_1 = 0.7$. An identical $9 \times 9 \times 15$ grid has been used in each method. Figure 5 compares the heat flux

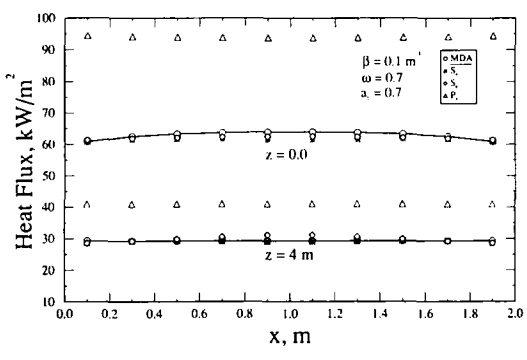

FIG. 5. Behavior of improved MDA method in optically thin limit.

profiles calculated by various methods. As expected, the P_1 approximation performs poorly in this limit. MDA has the accuracy of S_4 since the S_4 technique has been used for solving the G_s equation that does not contain the in-scattering or the medium emission terms. MDA would have the accuracy of S_6 in this limit if the S_6 technique was used for solving the G_s equation.

(b) In the optically thick limit, the G_m field provides the correct solution to the radiation transport equation. As shown in Fig. 6, P_1, MDA and discrete ordinate methods have comparable accuracies in this limit.

(c) From the discussions in Sections 5, 6a and 6b, we conclude that MDA is superior to higher-order moment methods (P_N) and as accurate as discrete-ordinate methods (S_N).

(d) As discussed in Section 3 and 4, direct evaluation of multiple integrals encountered in the solution of equation (2) presents a formidable task. The evaluation process is considerably simplified by use of Tucker's exponential correlation for surface–surface and volume–surface exchange coefficients. In spite of this simplification, G_s solution is computationally intensive and increasingly inefficient as the grid system is refined (see Table 3). One way of circumventing this computational difficulty is to seek an alternative formulation, such as the discrete-ordinate method, for solving the G_s equation. The resultant saving in computer time is well documented in Table 3.

(e) For the problem and grid system outlined in Section 6a, Table 4 compares the CPU times taken by different methods: P_1, MDA using Tucker's correlations for G_s, improved MDA based on S_4 for G_s, S_4 and S_6. In each method, the same convergence criterion, namely relative change in G_s and G_m, and I smaller than 10^{-4}% between iterations, is used. Improved MDA (P_1+S_4) is seen to be considerably faster than the equivalent discrete-ordinate method, S_4, especially at large β. On an IBM RISC 6000 workstation, S_4 solution takes 178.3 s for $\beta = 2$ m^{-1}, whereas improved MDA requires 7.7 s, of which 1.1 s is spent on the P_1 method for G_m and 6.6 s on S_4 for G_s. The economy of computer time is particularly impressive when the gas temperature field is unknown. For example, if 10 iterations are needed to solve the energy equation for the gas temperature field, the CPU time required by S_4 would be 1783 s. In MDA,

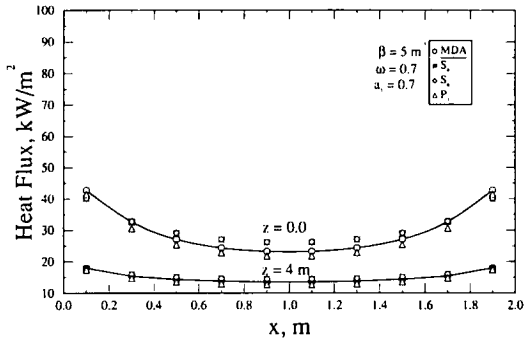

FIG. 6. Behavior of improved MDA method in optically thick limit.

G_s would need to be solved only once, requiring 6.6 s of CPU time, and all the iterations on the G_m field would be carried out using P_1. Thus the total CPU time incurred would be $6.6+10\times1.1 = 17.6$ s—merely one-hundredth of the resources required by S_4. S_4 for G_s generally requires only a fraction of the CPU time needed by S_4 for a complete radiation field. For example, it takes 6.6 s to determine the G_s field by S_4 when $\beta = 2$ m^{-1} as compared to 178.3 s for complete radiation field by S_4. The economy of computer time is realized in part from fewer iterations (eight vs 81) required by S_4-G_s to converge. Faster convergence results from the absence of medium emission and scattering terms in equation (2). The considerable saving in computer time also derives from not having to perform the in-scattering summation at each interior grid point.

(f) Generally, the discrete-ordinate method numerics have a characteristic of increasing CPU time with β. The improved MDA displays the opposite trend. The numerical difficulty at small β arises from the slow convergence of TDMI applied to G_m equations. A sparse matrix equation solver, such as YSMP, has been found to be 10–100 times faster than the TDMI algorithm. Moreover, the CPU time of the direct equation solver is independent of β. However, the computer memory requirement of YSMP increases non-linearly with the number of grids, making it almost impractical for grids larger than $10\times10\times10$. Further work is required to improve the convergence behavior of the G_m finite difference equations for the optically thin limit.

Table 4. Comparison of CPU times (s) on IBM RS/6000-550 workstation: $9\times9\times15$ grid, double precision arithmetic, relative convergence of 10^{-4}%

	$\omega = 0.1$			$\omega = 0.5$			$\omega = 0.9$		
β (m^{-1})	0.1	0.5	2.0	0.1	0.5	2.0	0.1	0.5	2.0
S_4	35.3	59.5	178.3						
S_6	746.9	775.3	1113.1	746.9	775.2				1113.2
MDA	132.3	110.0	90.8						
Improved MDA (S_4+P_1)	16.9	9.6	7.7	16.4					7.6
P_1	11.8	2.9	1.1		2.9			2.7	

REFERENCES

1. D. B. Olfe, A modification of the differential approximation for radiative transfer, *AIAA J.* **5,** 638–643 (1967).
2. D. B. Olfe, Application of a modified differential approximation to radiative transfer in a gray medium between concentric spheres and cylinders, *J. Quant. Spectrosc. Radiat. Transfer* **8,** 899–907 (1968).
3. D. B. Olfe, Radiative equilibrium of gray medium in a rectangular enclosure, *J. Quant. Spectrosc. Radiat. Transfer* **13,** 881–895 (1973).
4. M. F. Modest, Modified differential approximation for radiative transfer in general three-dimensional media, *J. Thermophys.* **3**(3), 283–288 (1989).
5. R. J. Tucker, Direct exchange areas for calculating radiation transfer in rectangular furnaces, *J. Heat Transfer* **108,** 707–710 (1986).
6. M. P. Mengüc and R. Viskanta, Radiative transfer in three-dimensional enclosures containing inhomogeneous, anisotropically scattering media, *J. Quant. Spectrosc. Radiat. Transfer* **33**(6), 533–549 (1985).
7. J. S. Truelove, Three-dimensional radiation in absorbing–emitting–scattering media using the discrete-ordinates approximation, *J. Quant. Spectrosc. Radiat. Transfer* **39**(1), 27–31 (1988).